ARTICLE IN PRESS

Available online 19 September 2019, 519 (2019) 705-713

主論文

Biochemical and Biophysical Research Communications xxx (xxxx) xxx

Contents lists available at ScienceDirect

Biochemical and Biophysical Research Communications

journal homepage: www.elsevier.com/locate/ybbrc

Smarcb1 maintains the cellular identity and the chromatin landscapes of mouse embryonic stem cells

Megumi Sakakura [a, b], Sho Ohta [a], Masaki Yagi [a, b], Akito Tanaka [b], Jo Norihide [b], Knut Woltjen [b], Takuya Yamamoto [b, c, d, e], Yasuhiro Yamada [a, b, c, *]

[a] Division of Stem Cell Pathology, Center for Experimental Medicine and Systems Biology, Institute of Medical Science, University of Tokyo, Tokyo, 108-8639, Japan
[b] Department of Life Science Frontiers, Center for iPS Cell Research and Application (CiRA), Kyoto University, Kyoto, 606-8507, Japan
[c] AMED-CREST, AMED 1-7-1 Otemachi, Chiyodaku, Tokyo, 100-0004, Japan
[d] Institute for the Advanced Study of Human Biology (WPI-ASHBi), Kyoto University, Yoshida-Konoe-cho, Sakyo-ku, Kyoto, 606-8501, Japan
[e] Medical-risk Avoidance based on iPS Cells Team, RIKEN Center for Advanced Intelligence Project (AIP), Kyoto, 606-8507, Japan

ARTICLE INFO

Article history:
Received 6 August 2019
Accepted 13 September 2019
Available online xxx

Keywords:
Smarcb1
Embryonic stem cell
Pluripotency
Trophectoderm
Chromatin accessibility

ABSTRACT

ES cell (ESC) identity is stably maintained through the coordinated regulation of transcription factors and chromatin structure. SMARCB1, also known as INI1, SNF5, BAF47, is one of the subunits of SWI/SNF (BAF) complexes that play a crucial role in regulating gene expression by controlling chromatin dynamics. Genetic ablation of *Smarcb1* in mice leads to embryonic lethality at the peri-implantation stage, indicating that *Smarcb1* is important for the early developmental stages. However, the role of SMARCB1 in the maintenance of the ESC identity remains unknown. Here we established mouse ESCs lacking *Smarcb1* and investigated the effect of *Smarcb1* ablation on the differentiation propensity of ESCs. We found an increased expression of trophectoderm-related genes including *Cdx2* in *Smarcb1*-deficient ESCs. Consistently, they exhibited an extended differentiation propensity into the trophectoderm lineage cells in teratomas. However, although *Smarcb1*-deficient cells were infrequently incorporated into the trophectoderm cell layer of blastocysts, they failed to contribute to mature placental tissues *in vivo*. Furthermore, *Smarcb1*-deficient cells exhibited a premature differentiation in the neural tissue of E14.5 chimeric embryos. Notably, we found that binding motifs for CTCF, which is involved in the maintenance of genomic DNA architecture was significantly enriched in chromatin regions whose accessibility was augmented in *Smarcb1*-deficient cells, while those for pluripotency factors were overrepresented in regions which have more closed structure in those cells. Collectively, we propose that SMARCB1-mediated remodeling of chromatin landscapes is important for the maintenance and differentiation of ESCs.

1. Introduction

In mammals, the first lineage segregation occurs at the preimplantation stage when totipotent blastomeres differentiate into either pluripotent inner cell mass (ICM) or trophectoderm. ESCs are derived from the ICM of the blastocyst and thus harbor differentiation ability into all cell lineages except for trophectoderm lineage. The maintenance of such pluripotency in self renewing ESCs is governed by the coordinated regulation of transcription factor network and chromatin structure [1–3].

Chromatin remodeling complexes, consisting of multiple subunits, utilize the energy of ATP hydrolysis to alter the distribution of nucleosomes, which subsequently modulates access of transcription factors to chromosomal DNA [4–7]. Among such chromatin remodelers, one of the most extensively analyzed complexes in ESCs is the SWI/SNF (BAF) subfamily [8]. Previous studies demonstrated that SMARCB1, a core component of the BAF complex, plays an important role in early mouse development [4]. In the present study, we examined the effect of *Smarcb1* ablation on the differentiation propensity of ESCs. We applied the CRISPR/Cas9-mediated genetic disruption in pre-existing ESC lines, and

* Corresponding author. Division of Stem Cell Pathology, Center for Experimental Medicine and Systems Biology, Institute of Medical Science, University of Tokyo, 4-6-1, Shirokanedai, Minato-ku, Tokyo, 108-8639, Japan.
E-mail address: yasu@ims.u-tokyo.ac.jp (Y. Yamada).

https://doi.org/10.1016/j.bbrc.2019.09.054
0006-291X/

succeeded to establish *Smarcb1*-deficient mouse ESCs. *Smarcb1*-deficient ESCs showed extended differentiation propensity for committing to the trophectoderm lineage as well as the three different germ layers in teratomas. However, these cells exhibited impaired differentiation during embryonic development *in vivo*. These results highlight an important role of *Smarcb1* in the maintenance of the mouse ESC identity.

2. Materials and methods

Detailed experimental procedures are provided in supplementary experimental procedures.

2.1. Culture and maintenance of ESCs

V6.5 and KH2 mouse ESCs were maintained on feeders in knockout DMEM with 2 mM L-glutamine, 100 × NEAA, 100 U/ml penicillin, 100 μg/ml streptomycin (P/S), 15% Fetal Bovine Serum (FBS), 0.11 mM β-mercaptoethanol and 1000 U/ml human recombinant leukemia inhibitory factor (LIF) [9].

2.2. Establishment of Smarcb1 knockout ESCs

In V6.5 cells, cells were transfected with 5 μg of px330-PGK-puro-pA containing sgRNA sequence targeting *Smarcb1*. After the selection, colonies were picked up and expanded. Each clone was evaluated by Sanger sequencing and immunoblotting. In KH2 cells, the knockout cell lines were generated as previously described [10,11].

2.3. In vivo experiment

All animal experiments were approved by the CiRA Animal Experiment Committee and IMSUT Animal Experiment Committee, and the care of the animals was in accordance with institutional guidelines. For teratoma formation, ESCs were trypsinized for single-cell suspension and 1×10^6 or 2×10^6 cells were injected subcutaneously into BALB/cSlc-nu/nu mice. For chimera formation, EGFP-labelled ES cells were injected into the E2.5 (8 cell) or blastocoels of E3.5 blastocysts. Injected blastocysts were transferred into the uteri of pseudo-pregnant ICR mice [12].

2.4. HE staining and immunohistochemistry

Samples were fixed with 4% paraformaldehyde overnight at room temperature and embedded in paraffin as described previously [13]. Sections were stained with haematoxylin and eosin (HE). For immunohistochemistry, sections were treated with Histofine (Nichirei). After rinsing with PBS, sections were incubated with anti-GFP antibody (Abcam, ab183734; dilution 1:200), anti-NESTIN antibody (BD, 611658; dilution 1:400) or anti-PL-1antibody (Santa Crus Biotechnology, sc-34713; dilution 1:150) overnight at 4 °C. Sections were then rinsed with PBS and incubated with Histofine Simple Stain Mouse MAX PO (Nichirei) containing secondary antibody for 30 min at room temperature. DAB Substrate Kit (Nichirei) was used for detection. For immunofluorescence staining, anti-GFP antibody (Abcam, ab13970; dilution 1:500) and anti-TPBPA antibody (Abcam, ab104401; dilution 1:200) were used as primary antibodies.

2.5. FACS sorting

For RNA-seq and ATAC-seq analyses, ESCs were sorted by a fluorescence activated cell sorter (FACS) Aria II (BD). Alexa Flour 647 conjugated anti-SSEA1 antibody (Santa Cruz, sc-21702 AF647 clone MC480 or BD Pharmingen, Clone MC480, cat: 562277) was used for the sorting. Sorted cells were used for RNA isolation and library preparation for next generation sequencing.

2.6. Quantitative RT-PCR and immunoblotting

Quantitative RT-PCR was performed using GoTaq qPCR Master Mix and CXR Reference Dye (Promega). StepOnePlus Real-Time PCR system (Applied Biosystems) was used. For Western blotting, feeder cells were removed by culturing in 2i/LIF ES medium which was supplemented with 1 μM PD0325901 (STEMGENT) and 3 μM CHIR99021 (STEMGENT) [9]. The primary antibodies used were anti-INI1/SNF5 (Sigma-Aldrich:SAB4200202) and anti-β-actin (Santa Cruz, sc-47778). Protein bands were visualized with Pierce ECL plus Western Blotting Substrate (Thermo Scientific) and detected by LAS4000 (GE Healthcare).

2.7. RNA-seq analysis and ATAC-seq analysis

For RNA-seq, 200 ng of high-quality RNA was used for the library preparation. RNA-seq libraries were generated using Truseq Stranded mRNA LT sample prep kit (Illumina) [9]. Resulting RNA-seq libraries were single-end sequenced with a length of 75 bp on NextSeq 500 (Illumina).

ATAC-seq libraries were prepared as previously described with some modifications [14]. Cells were collected by FACS with a SSEA-1 antibody (see the section above) and 50,000 cells were used to prepare ATAC-seq libraries. The libraries were paired-end sequenced with a length of 50 bp on Nextseq 500.

2.8. Data availability

All the RNA-seq and ATAC-seq data are available in SRA (BioProject: PRJNA551543).

3. Results

3.1. Derivation of Smarcb1-deficient ESCs

Previous studies demonstrated that ESCs cannot be derived from embryos deficient in *Smarcb1* [15,16]. Therefore, in the present study, we aimed to establish *Smarcb1* knockout (KO) ESCs by genetic manipulation of pre-existing ESC lines. We took two different approaches for this purpose. First, we employed a conditional genome editing system we have reported previously [11,17]. A doxycycline (Dox)-responsive promoter with the *Cas9* gene was introduced into downstream of the *Col1a1* locus in KH2 ESCs which contain *M2-rtTA* under control of the *Rosa26* promoter (Fig. S1) [11]. An sgRNA that targets *Smarcb1* was introduced using a *piggyBac* transposon vector. In the second approach, *Cas9* and an sgRNA were transiently expressed in V6.5 ESCs using a plasmid vector. In both approaches, we obtained multiple ESC clones that exhibit out-of-frame mutations at the *Smarcb1* locus (Figure S1A, S1B and S1C). Consistent with the genetic mutations, SMARCB1 was not detectable by immunoblotting in these cells (Fig. 1A), indicating successful generation of *Smarcb1* KO ESCs.

The proliferation rate of *Smarcb1*-deficient ESCs was slower than that of control ESCs (Fig. 1B). To examine differentiation status of *Smarcb1*-deficient ESCs, we next examined their morphology and the activity of alkaline phosphatase (ALP), a marker of undifferentiated ESCs. Although *Smarcb1*-deficient ESC clones could be propagated more than 20 passages, a subset of *Smarcb1* KO ESC colonies did not clearly show defined margins of cells and exhibited a fuzzy appearance (Fig. 1C). In addition, ESC colonies with a fuzzy appearance often showed a reduced staining for ALP activity

Please cite this article as: M. Sakakura et al., Smarcb1 maintains the cellular identity and the chromatin landscapes of mouse embryonic stem cells, Biochemical and Biophysical Research Communications, https://doi.org/10.1016/j.bbrc.2019.09.054

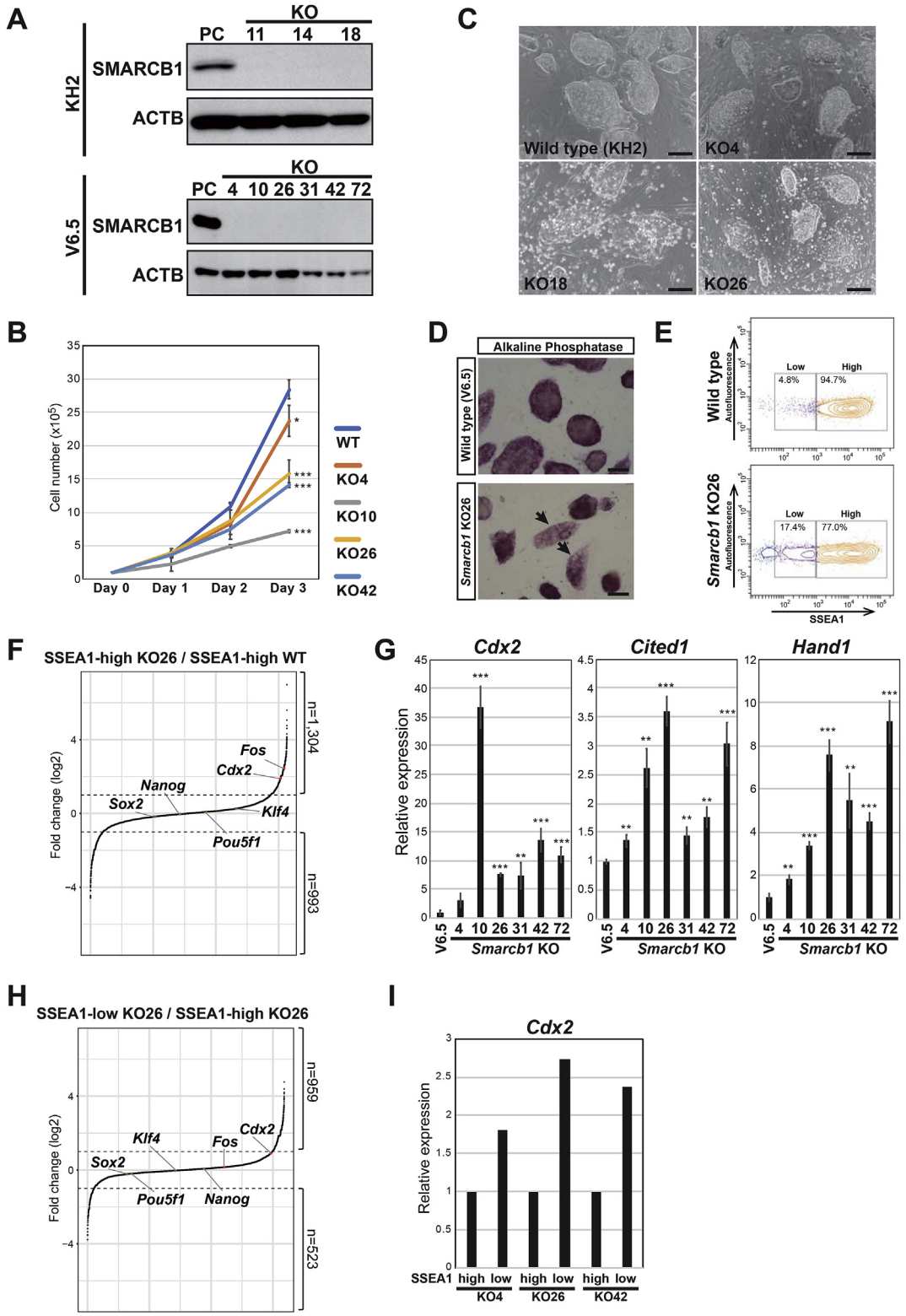

Fig. 1. Derivation of *Smarcb1*-deficient ESCs and their gene expression profiling
A: Immunoblotting analysis for SMARCB1. No detectable expression of SMARCB1 was observed in *Smarcb1*-deficient ESCs.B: Cell growth assay of *Smarcb1*-deficient ESCs (*$p < 0.05$; ***$p < 0.001$, student *t*-test). Error bars represent SD of three independent experiments.C: Representative morphology of *Smarcb1*-deficient ESCs and control wild-type ESCs. Scale bars, 100 μm. D: Staining for Alkaline phosphatase. Arrows indicate colonies with a reduced staining for ALP activity. Scale bars: 100 μm E: Flow cytometry plots following staining with SSEA1 antibody. Note that a subset of *Smarcb1*-deficient ESCs exhibit lower levels of SSEA1 while the majority of control wild type ESCs show higher levels of SSEA1. F: RNA-seq analysis. SSEA1-high *Smarcb1*-deficient ESCs (KO26) were compared with SSEA1-high wild-type ESCs. Fold changes of normalized counts (*Smarcb1*-deficient ESCs/wild-type ESCs) are shown in log2 scale. G: qRT-PCR analysis for *Cdx2*, *Cited1* and *Hand1* in *Smarcb1*-deficient and control ESCs (V6.5). Data are presented as the mean ± SD of biological triplicates. The mean expression level of control ESCs was set to 1. H: RNA-seq analysis of *Smarcb1*-deficient ESCs (KO26). SSEA1-low cells were compared with SSEA1-high cells. Fold changes of normalized counts (SSEA1-low cells/SSEA1-high cells) are shown in log2 scale. I: qRT-PCR analysis for *Cdx2* in *Smarcb1*-deficient SSEA1-high and SSEA1-low ESCs. Data are presented as the mean of technical triplicates. The expression level in SSEA1-high samples in each KO cells was set to 1.

Please cite this article as: M. Sakakura et al., Smarcb1 maintains the cellular identity and the chromatin landscapes of mouse embryonic stem cells, Biochemical and Biophysical Research Communications, https://doi.org/10.1016/j.bbrc.2019.09.054

(Fig. 1D). Together, these results suggest that loss of SMARCB1 impairs the maintenance of the undifferentiated state of ESCs.

3.2. Global gene expression profiling of Smarcb1-deficient ESCs

To address molecular mechanisms by which *Smarcb1*-deficient ESCs exhibits impaired maintenance of the undifferentiated state, we next performed RNA-seq to examine global gene expression. In this analysis, to exclude the effect of differentiated population of *Smarcb1*-deficient ESCs on gene expression profiling, we first enriched undifferentiated cells by fluorescence-activated cell sorting (FACS) with SSEA1 antibody staining. Consistent with the reduced ALP activity, a subset of *Smarcb1* KO ESCs showed decreased levels of SSEA1 expression whereas the majority of control ESCs displayed higher levels of SSEA1 expression (Fig. 1E). Therefore, we compared gene expression profiles of SSEA1-high *Smarcb1* KO ESCs with SSEA1-high control ESCs (V6.5). Notably, expression of *Nanog*, *Pou5f1* and *Sox2*, key transcription factors comprising the core gene regulatory network in ESCs, was not prominently reduced in *Smarcb1* KO ESCs (Figs. 1F and S1D) [2,3], suggesting that impaired maintenance of undifferentiated state is not attributable to decreased expression of key pluripotency genes in ESCs. In contrast, we identified 2297 genes that are differentially expressed between *Smarcb1* KO ESCs and control ESCs (>2 folds difference; 1304 upregulated genes and 993 downregulated genes) (Fig. 1F), indicating that *Smarcb1* ablation indeed has an impact on global gene expression in undifferentiated ESCs.

3.3. Increased expression of genes related to placenta development in Smarcb1-deficient ESCs

We found that *Fos*, which regulates trophoblast-specific gene expression [18], as well as *Cdx2*, which plays a critical role in trophectoderm differentiation [19], was upregulated in SSEA1-high *Smarcb1* KO ESCs when compared with SSEA1-high wild-type ESCs (Fig. 1F). Consistently, qRT-PCR analyses using multiple clones revealed that *Cdx2*, *Cited1* and *Hand1*, which are associated with trophectoderm differentiation are upregulated in *Smarcb1* KO ESCs when compared with control wild type ESCs (Fig. 1G). To further investigate initial differentiation of *Smarcb1*-deficient ESCs, we next compared the gene expression profile of SSEA1-low population with that of SSEA1-high population among *Smarcb1* KO ESCs. The comparison identified 1482 genes that are differentially expressed between SSEA1-high and SSEA1-low cells (>2 fold difference; 959 upregulated genes and 523 downregulated genes) (Fig. 1H). Notably, increased expression of *Cdx2* was confirmed in SSEA1-low *Smarcb1* KO ESCs when compared with SSEA1-high cells of the corresponding clones (Fig. 1H and I).

3.4. Extended differentiation propensity of Smarcb1-deficient ESCs in teratomas

As we mentioned above, a couple of genes related to placental development, e.g. *Cdx2* and *Fos,* were identified as genes that are upregulated by loss of *Smarcb1*. This observation prompted us to investigate the effect of the altered gene expression patterns in *Smarcb1*-deficient ESCs on differentiation propensity. We first examined expression of CDX2 in ESCs at the protein level. Immunofluorescence for CDX2 revealed that *Smarcb1*-deficient ESC colonies often contain small clusters of CDX2-positive cells even in the presence of LIF and feeder cells, which is hardly detected in wild-type ESCs (Fig. 2A). CDX2-positive cells did not express OCT4 (Fig. 2A), which is in accordance with previous findings demonstrating the reciprocal repression of ICM-specific factor OCT4 and trophectoderm-specific factor CDX2 [19]. We next performed a teratoma assay by inoculating ESCs into the subcutaneous tissue of immunocompromised mice. Despite of the expression changes, *Smarcb1* KO ESCs efficiently developed teratomas and no significant difference was observed in efficiency of teratoma formation or size of teratomas when compared with control ESCs (data is not shown). A histological analysis revealed that *Smarcb1*-deficient ESCs give rise to various cell types including cartilage tissue, neuronal tissue and glandular tissue (Figs. 2B and S2A), suggesting that loss of *Smarcb1* does not compromise pluripotency. Of note, teratomas often contain small clusters of trophoblast-like giant cells (>3 cells/high power field [x400]), which are positive for PL-1 expression, a marker for trophoblast cells (Fig. 2C and D), indicating that *Smarcb1*-deficient ESCs are capable of differentiating into trophectoderm lineage cells as well as derivatives of three germ layers at least in teratomas. Together with the increased expression of placenta development-related genes, these results suggest that loss of *Smarcb1* confers the extended differentiation capacity on ESCs.

3.5. Impaired differentiation potential of Smarcb1-deficient ESCs in vivo

We next investigated the differentiation potential of *Smarcb1*-deficient ESCs *in vivo*. For that purpose, we injected EGFP-labelled *Smarcb1* KO ESCs into 8-cell stage embryos (E2.5) and examined these embryos at blastocyst stage (E3.5) (Fig. 3A). We found that EGFP-positive *Smarcb1* KO cells resided mainly at the ICM region of the blastocysts (Fig. 3A and B). EGFP-positive cells were also observed in the trophectoderm layer of blastocytes, albeit at low frequencies (Fig. 3C). Consistent with this, a small subset of blastocysts exhibited co-localized expression of EGFP and CDX2 in the trophectoderm layer of the blastocyst (Fig. 3D). However, no significant differences in the frequency of EGFP-positive cells in the trophectoderm layer were observed in blastocysts after injection of *Smarcb1* KO and wild type ESCs (Fig. 3C). These results suggest that, although *Smarcb1*-deficient ESCs infrequently contribute to the trophectoderm layer of the blastocyst, they basically lack the extended differentiation propensity into trophectoderm lineage cells in an *in vivo* context.

To further examine differentiation potential of *Smarcb1*-deficient cells at a subsequent stage of embryonic development *in vivo*, we injected EGFP-labelled *Smarcb1* KO ESCs into blastocyst stage embryos (E3.5) and transferred these embryos in the uterus of pseudopregnant mice (Fig. 3E). Then these conceptuses at E14.5 were analyzed for histology and EGFP expression (Fig. 3E). In the placenta of conceptus at E14.5, EGFP-positive cells were observed only in fetal capillary endothelium (Fig. 3F and G). However, trophectoderm-derived placenta cells, such as spongiotrophoblast cells and trophoblast giant cells never showed EGFP expression (Fig. 3G). Moreover, EGFP-positive cells in the placenta did not express TPBPA, which is a marker for trophoblast precursors and spongiotrophoblast cells (Fig. 3H). Collectively, we conclude that *Smarcb1*-deficient ESCs do not differentiate into mature trophectoderm derivatives *in vivo*.

In contrast to the absence of EGFP-positive cells in trophectoderm derivatives, we observed EGFP-positive KO cells in various organs in E14.5 chimeric embryos, including the cartilage tissue, the central nervous system (CNS) tissue, and the glandular tissue (Fig. 3F, S3 and 4A), affirming that *Smarcb1*-deficient cells differentiate into three germ layers *in vivo* and that *Smarcb1*-deficient ESCs retain pluripotency. However, we found that the number of Nestin-expressing neural progenitor cells decreases in EGFP-positive areas in the brain and spinal cord of E14.5 chimeric embryos (Fig. 4B). These findings suggest that *Smarcb1* KO cells exhibit premature differentiation in CNS tissue, which is consistent with previous findings that *Brg1* is required for the self-renewal of

Please cite this article as: M. Sakakura et al., Smarcb1 maintains the cellular identity and the chromatin landscapes of mouse embryonic stem cells, Biochemical and Biophysical Research Communications, https://doi.org/10.1016/j.bbrc.2019.09.054

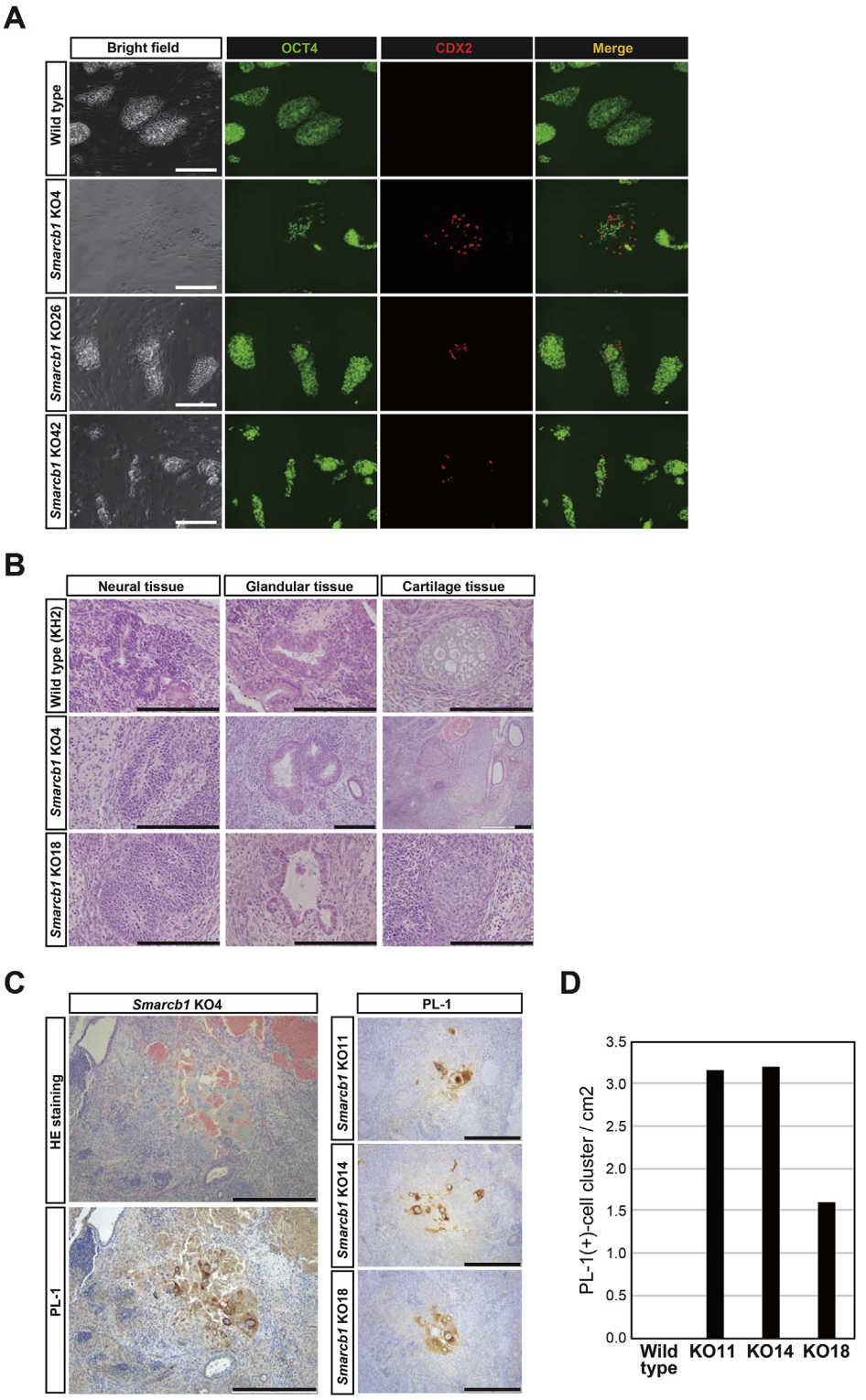

Fig. 2. Extended differentiation potential of *Smarcb1*-deficient ESCs in teratomas.
A: Immunofluorescent staining for OCT4 and CDX2 in *Smarcb1*-deficient ESCs. Scale bars: 200 μm. B: *Smarcb1* KO ESCs generated teratomas containing derivatives of three germ layers in the subcutaneous layer of immunocompromised mice. Scale bars: 200 μm. C: *Smarcb1* KO teratomas contain a cluster of trophoblast giant cells in hemorrhage region. Trophoblast giant cells exhibit positive staining for PL-1. Scale bars: 500 μm. D: Frequency of PL-1-positive clusters in *Smarcb1*-deficient teratomas.

Please cite this article as: M. Sakakura et al., Smarcb1 maintains the cellular identity and the chromatin landscapes of mouse embryonic stem cells, Biochemical and Biophysical Research Communications, https://doi.org/10.1016/j.bbrc.2019.09.054

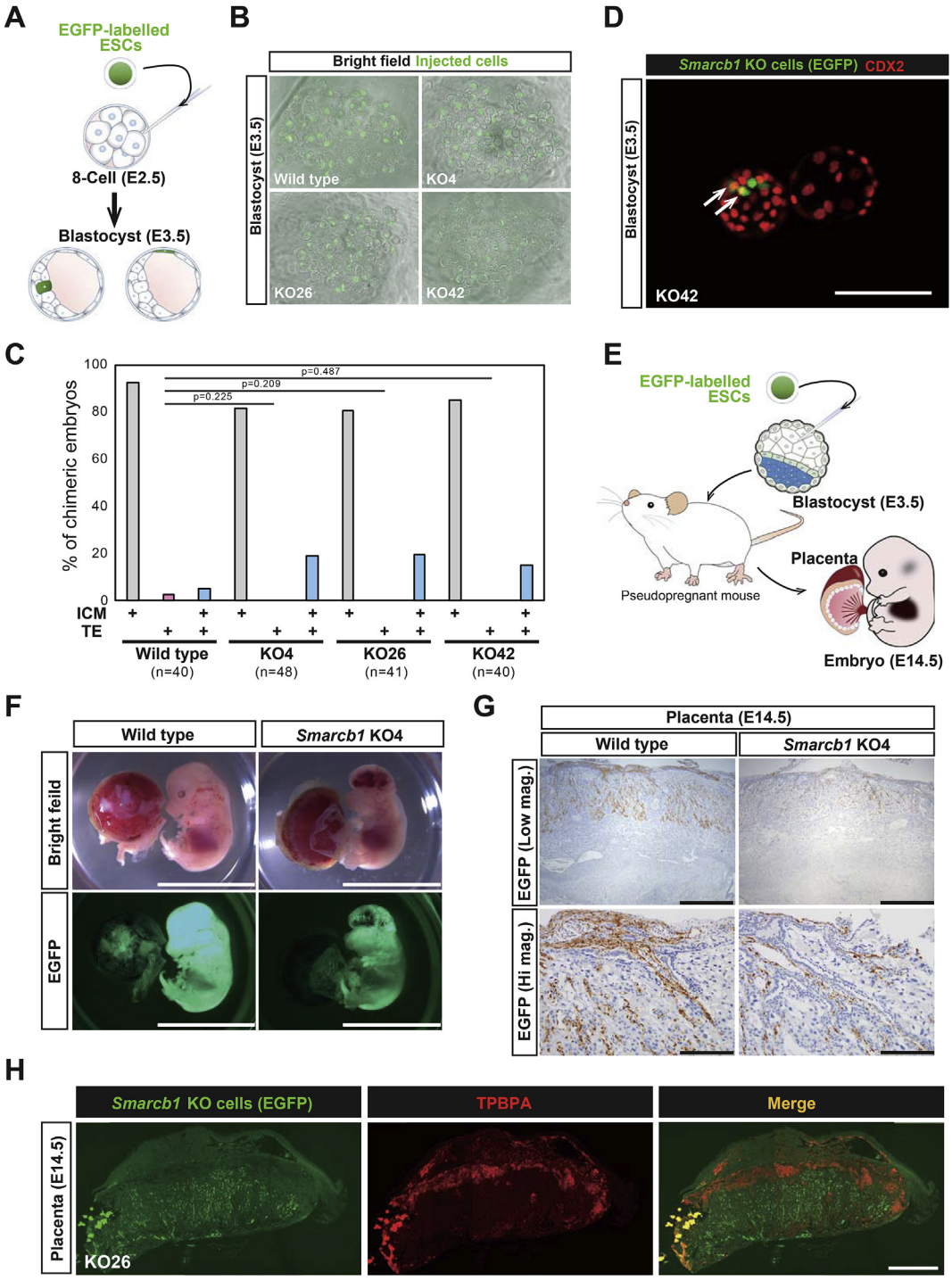

Fig. 3. Differentiation potential of *Smarcb1*-deficient ESCs.
A: Schematic illustration of experimental design. EGFP-labelled ESCs were injected into 8-cell stage embryos (E2.5) and analyzed at the blastocyst stage (E3.5). B: EGFP images of the blastocysts after injection of EGFP-labelled ESCs. C: Frequency of chimeric embryos with EGFP-positive cells at ICM and the trophectoderm (TE) layer (p-value, Fisher's exact test). D: Immunofluorescent staining for CDX2. Note that EGFP-positive cells simultaneously express CDX2 (arrows). Scale bar: 100 μm. E: Schematic illustration of experimental design. EGFP-labelled *Smarcb1* KO ESCs were injected into blastocysts (E3.5). These embryos were transferred into the uterus of pseudopregnant mice. Conceptuses at E14.5 were analyzed for histology and EGFP expression. F: EGFP images of the embryo and placenta at E14.5. Scale bars: 10 mm. G: Immunohistochemistry for EGFP of the placenta. EGFP positive cells are observed only in fetal capillary endothelium. Scale bars: 1 mm (upper), 200 μm (lower). H: Immunohistochemistry for EGFP and TPBPA of the placenta. EGFP positive cells do not express TPBPA. Scale bar: 1 mm.

Please cite this article as: M. Sakakura et al., Smarcb1 maintains the cellular identity and the chromatin landscapes of mouse embryonic stem cells, Biochemical and Biophysical Research Communications, https://doi.org/10.1016/j.bbrc.2019.09.054

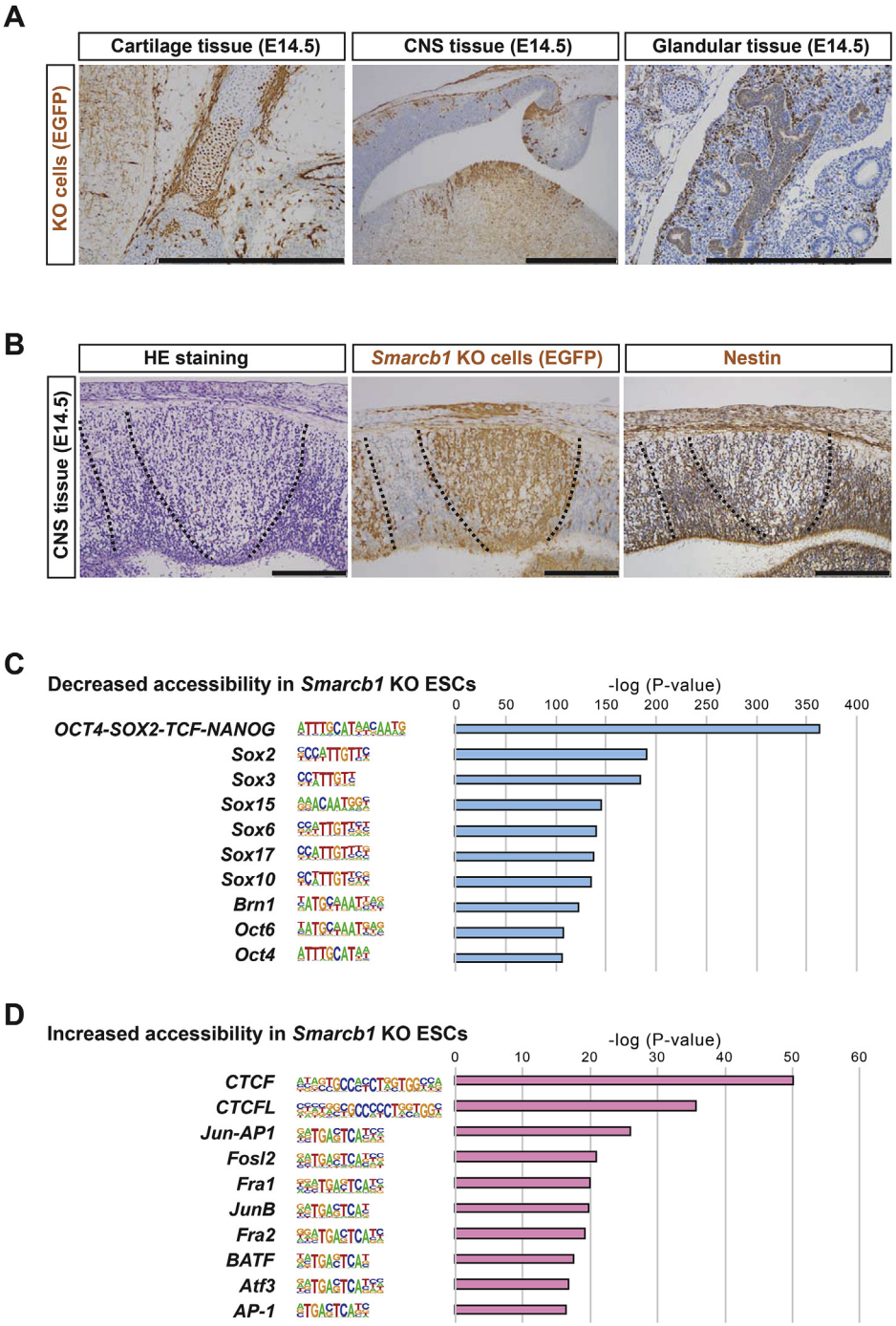

Fig. 4. Impaired differentiation and altered chromatin accessibility in *Smarcb1*-deficient ESCs.
A: Immunohistochemistry for EGFP of various tissues in the E14.5 embryo. Scale bars: 500 μm. B: Immunohistochemistry for EGFP of the CNS tissue. Note that Nestin expression is reduced in EGFP-positive CNS cells. Scale bars: 200 μm. C: ATAC-seq analysis revealed that binding motifs for OCT4 and SOX2 were significantly overrepresented in regions which have more closed structure in *Smarcb1* KO ESCs. D: CTCF binding motifs, as well as AP-1-related motifs, were significantly enriched in chromatin regions whose accessibility was augmented in *Smarcb1*-deficient cells in the ATAC-seq analysis.

neural progenitor cells [20]. Together, *Smarcb1* is required for proper ectoderm differentiation of embryonic cells.

3.6. Altered chromatin accessibility in Smarcb1-deficient ESCs

Finally, to gain mechanistic insights into the biased and impaired differentiation potential of *Smarcb1*-deficient ESCs, we assessed changes in genome-wide chromatin accessibility by Assay for Transposase-Accessible Chromatin Sequencing (ATAC-seq). To exclude the secondary effect of the altered differentiation status on the analysis, we compared SSEA1-high, undifferentiated *Smarcb1* KO ESCs with SSEA1-high wild-type ESCs. First, we examined ATAC-seq signals at gene promoter regions. Expectedly, changes in the signal intensity at promoter regions were found to be correlated with gene expression alteration of corresponding genes, which supports the validity and reliability of the ATAC-seq analysis. Then,

Please cite this article as: M. Sakakura et al., Smarcb1 maintains the cellular identity and the chromatin landscapes of mouse embryonic stem cells, Biochemical and Biophysical Research Communications, https://doi.org/10.1016/j.bbrc.2019.09.054

we attempted to identify genomic regions whose accessibility was altered in the *Smarcb1*-deficient cells. We identified 77 ATAC-seq peaks 806 peaks which were upregulated and downregulated in *Smarcb1*-deficient ESCs, respectively. We found that binding motifs for OCT4 and SOX2, which are core pluripotency transcription factors, were significantly enriched at open chromatin regions downregulated in *Smarcb1*-deficient ESCs (Fig. 4C), which is consistent with our observation that *Smarcb1*-deficient ESCs prone to differentiate. In contrast, a CTCF motif was overrepresented in open chromatin regions upregulated in *Smarcb1* KO ESCs (Fig. 4D). Given that CTCF is an insulator-binding protein and mediates functional chromatin interactions in ESCs [21,22], our results suggest that SMARCB1-mediated chromatin remodeling is important for the nuclear organization, which is essential for proper maintenance and differentiation of mESCs. We also found that AP-1 related motifs are overrepresented at open chromatin regions in *Smarcb1* KO ESCs (Fig. 4D), which supports the assumption that Fos-mediated regulation of trophoblast-specific genes is involved in the biased differentiation into the trophectoderm lineage.

4. Discussion

Here we established *Smarcb1*-deficient mouse ESCs and found that these ESCs exhibited impaired maintenance of the undifferentiated state. Notably, expression levels of core transcription factors, *Pou5f1*, *Nanog* and *Sox2*, which are required for the stable maintenance of the ESC identity, were not significantly affected in *Smarcb1*-deficient ESCs. However, we found that binding motifs for OCT4 and SOX2 were significantly enriched in chromatin regions whose accessibility was downregulated in these cells. Previous ChIP-Seq studies revealed that the esBAF complex binds to genes that are transcriptional targets of OCT4, SOX2 and NANOG in ESCs [8,23]. These results suggest that SMARCB1-mediated chromatin remodeling activity may ensure the function of key pluripotency transcription factors. We also found that binding motifs of CTCF, which has been implicated as a key genome organizer during development [21,22], are enriched in open chromatin regions in *Smarcb1*-deficient ESCs. Collectively, our results highlight a critical role of epigenetic regulation in the maintenance of unique properties of ESCs.

Consistent with the fact that ICM gives rise to fetal tissues but does not differentiate into trophectoderm, ICM-derived ESCs generally do not differentiate into trophectoderm lineage cells. However, we found that *Smarcb1*-deficient ESCs readily differentiate into CDX2-expressing cells *in vitro* and a subset of cells are able to contribute to the trophectoderm layer of the blastocyst. Notably, a previous study demonstrated that *BAF155*-depleted embryos have ectopic expression of *Nanog* in the trophectoderm layer cells, suggesting that the lineage commitment into trophectoderm cells is impaired in these embryos. Together, these results underscore the importance of BAF complexes in the maintenance of cellular identity after cell type specification during early development.

In summary, we established *Smarcb1*-deficient mouse ESCs and showed that *Smarcb1*-deficient ESCs exhibited impaired maintenance of the undifferentiated state but had extended differentiation capacity in teratomas. However, *Smarcb1*-deficient ESCs showed impaired ectoderm differentiation during embryonic development *in vivo*. We also found that *Smarcb1*-deficient ESCs harbor altered chromatin accessibility. We propose that *Smarcb1*-mediated regulation of chromatin structure and assembly plays a critical role in the maintenance of mouse ESC identity.

Acknowledgments

We thank K.Semi, H.Shibata, K.Mitsunaga, T. Ukai, R. Sakamoto, M. Kikuchi, M. Kabata and M. Baba for technical assistance. The authors were supported in part by AMED-CREST (JP18gm1110004); AMED P-CREATE (JP18cm0106203); JSPS KAKENHI (18H04026, 18J14965); Research Grants of Princess Takamatsu Cancer Research Fund; the Takeda Science Foundation; the Mochida Memorial Foundation for Medical & Pharmaceutical Research; and the Naito Foundation. The ASHBi is supported by World Premier International Research Center Initiative (WPI), MEXT, Japan.

Appendix A. Supplementary data

Supplementary data to this article can be found online at https://doi.org/10.1016/j.bbrc.2019.09.054.

References

[1] M.A. Surani, K. Hayashi, P. Hajkova, Genetic and epigenetic regulators of pluripotency, Cell 128 (2007) 747–762.
[2] R. Jaenisch, R. Young, Stem cells, the molecular circuitry of pluripotency and nuclear reprogramming, Cell 132 (2008) 567–582.
[3] G. Martello, A. Smith, The nature of embryonic stem cells, Annu. Rev. Cell Dev. Biol. 30 (2014) 647–675.
[4] L. Ho, G.R. Crabtree, Chromatin remodelling during development, Nature 463 (2010) 474–484.
[5] C.L. Peterson, I. Herskowitz, Characterization of the yeast SWI1, SWI2, and SWI3 genes, which encode a global activator of transcription, Cell 68 (1992) 573–583.
[6] J.W. Tamkun, R. Deuring, M.P. Scott, M. Kissinger, A.M. Pattatucci, T.C. Kaufman, J.A. Kennison, brahma: a regulator of Drosophila homeotic genes structurally related to the yeast transcriptional activator SNF2/SWI2, Cell 68 (1992) 561–572.
[7] H. Kwon, A.N. Imbalzano, P.A. Khavari, R.E. Kingston, M.R. Green, Nucleosome disruption and enhancement of activator binding by a human SW1/SNF complex, Nature 370 (1994) 477–481.
[8] L. Ho, J.L. Ronan, J. Wu, B.T. Staahl, L. Chen, A. Kuo, J. Lessard, A.I. Nesvizhskii, J. Ranish, G.R. Crabtree, An embryonic stem cell chromatin remodeling complex, esBAF, is essential for embryonic stem cell self-renewal and pluripotency, Proc. Natl. Acad. Sci. U. S. A. 106 (2009) 5181–5186.
[9] M. Yagi, S. Kishigami, A. Tanaka, K. Semi, E. Mizutani, S. Wakayama, T. Wakayama, T. Yamamoto, Y. Yamada, Derivation of ground-state female ES cells maintaining gamete-derived DNA methylation, Nature 548 (2017) 224–+.
[10] K. Ohnishi, K. Semi, T. Yamamoto, M. Shimizu, A. Tanaka, K. Mitsunaga, K. Okita, K. Osafune, Y. Arioka, T. Maeda, H. Soejima, H. Moriwaki, S. Yamanaka, K. Woltjen, Y. Yamada, Premature termination of reprogramming in vivo leads to cancer development through altered epigenetic regulation, Cell 156 (2014) 663–677.
[11] N. Jo, Y. Sogabe, Y. Yamada, T. Ukai, H. Kagawa, K. Mitsunaga, K. Woltjen, Y. Yamada, Platforms of in vivo genome editing with inducible Cas9 for advanced cancer modeling, Cancer Sci. 110 (2019) 926–938.
[12] H. Shibata, S. Komura, Y. Yamada, N. Sankoda, A. Tanaka, T. Ukai, M. Kabata, S. Sakurai, B. Kuze, K. Woltjen, H. Haga, Y. Ito, Y. Kawaguchi, T. Yamamoto, Y. Yamada, In vivo reprogramming drives Kras-induced cancer development, Nat. Commun. 9 (2018).
[13] Y. Terada, N. Jo, Y. Arakawa, M. Sakakura, Y. Yamada, T. Ukai, M. Kabata, K. Mitsunaga, Y. Mineharu, S. Ohta, M. Nakagawa, S. Miyamoto, T. Yamamoto, Y. Yamada, Human pluripotent stem cell-derived tumor model uncovers the embryonic stem cell signature as a key driver in atypical teratoid/rhabdoid tumor, Cell Rep. 26 (2019), 2608-+.
[14] J.D. Buenrostro, P.G. Giresi, L.C. Zaba, H.Y. Chang, W.J. Greenleaf, Transposition of native chromatin for fast and sensitive epigenomic profiling of open chromatin, DNA-binding proteins and nucleosome position, Nat. Methods 10 (2013) 1213–1218.
[15] A. Klochendler-Yeivin, L. Fiette, J. Barra, C. Muchardt, C. Babinet, M. Yaniv, The murine SNF5/INI1 chromatin remodeling factor is essential for embryonic development and tumor suppression, EMBO Rep. 1 (2000) 500–506.
[16] C.J. Guidi, A.T. Sands, B.P. Zambrowicz, T.K. Turner, D.A. Demers, W. Webster, T.W. Smith, A.N. Imbalzano, S.N. Jones, Disruption of Ini1 leads to peri-implantation lethality and tumorigenesis in mice, Mol. Cell. Biol. 21 (2001) 3598–3603.
[17] C. Beard, K. Hochedlinger, K. Plath, A. Wutz, R. Jaenisch, Efficient method to generate single-copy transgenic mice by site-specific integration in embryonic stem cells, Genesis 44 (2006) 23–28.
[18] K. Kubota, L.N. Kent, M.A. Rumi, K.F. Roby, M.J. Soares, Dynamic regulation of AP-1 transcriptional complexes directs trophoblast differentiation, Mol. Cell. Biol. 35 (2015) 3163–3177.
[19] H. Niwa, Y. Toyooka, D. Shimosato, D. Strumpf, K. Takahashi, R. Yagi, J. Rossant, Interaction between Oct3/4 and Cdx2 determines trophectoderm differentiation, Cell 123 (2005) 917–929.
[20] J. Lessard, J.I. Wu, J.A. Ranish, M. Wan, M.M. Winslow, B.T. Staahl, H. Wu,

R. Aebersold, I.A. Graef, G.R. Crabtree, An essential switch in subunit composition of a chromatin remodeling complex during neural development, Neuron 55 (2007) 201–215.

[21] L. Handoko, H. Xu, G. Li, C.Y. Ngan, E. Chew, M. Schnapp, C.W. Lee, C. Ye, J.L. Ping, F. Mulawadi, E. Wong, J. Sheng, Y. Zhang, T. Poh, C.S. Chan, G. Kunarso, A. Shahab, G. Bourque, V. Cacheux-Rataboul, W.K. Sung, Y. Ruan, C.L. Wei, CTCF-mediated functional chromatin interactome in pluripotent cells, Nat. Genet. 43 (2011) 630–638.

[22] J.E. Phillips, V.G. Corces, CTCF: master weaver of the genome, Cell 137 (2009) 1194–1211.

[23] L. Ho, R. Jothi, J.L. Ronan, K. Cui, K. Zhao, G.R. Crabtree, An embryonic stem cell chromatin remodeling complex, esBAF, is an essential component of the core pluripotency transcriptional network, Proc. Natl. Acad. Sci. U. S. A. 106 (2009) 5187–5191.

Please cite this article as: M. Sakakura et al., Smarcb1 maintains the cellular identity and the chromatin landscapes of mouse embryonic stem cells, Biochemical and Biophysical Research Communications, https://doi.org/10.1016/j.bbrc.2019.09.054

Sakakura et al.

Smarcb1 maintains the cellular identity and the chromatin landscapes of mouse embryonic stem cells

Inventory of Supplementary material

Supplementary experimental procedures

Culture and maintenance of ESCs

V6.5 and KH2 mouse ESCs were maintained on feeders (MEFs treated with mitomycin C [Kyowa Hakko Kirin Co., Ltd.]) in knockout DMEM (GIBCO) with 2 mM L-glutamine (Nacalai tesque), 100×NEAA (Nacalai tesque), 100 U/ml penicillin, 100 μg/ml streptomycin (P/S) (Nacalai tesque), 15% Fetal Bovine Serum (FBS) (GIBCO), 0.11 mM β-mercaptoethanol (GIBCO) and 1000 U/ml human recombinant leukemia inhibitory factor (LIF) (Wako).

Establishment of *Smarcb1* knockout ESCs

In V6.5 cells, the knockout cell lines were generated as previously described. Briefly, px330-PGK-puro-pA was generated based on pX330-U6-Chimeric_BB-CBh-hSpCas9 (Addgene plasmid no. 42230) [1]. sgRNA was ligated with px330-PGK-puro-pA. sgRNA sequence targeting *Smarcb1* was GACGGGGAGTTCTACATGAT. Cells were transfected with 5 μg of the plasmid using Xfect mES cell Transfection Reagent (Clontech) and selected using 1.25 μg ml $^{-1}$puromycin (Sigma) for 1.5 days. After the selection, colonies were picked up and expanded. Each clone was evaluated by Sanger sequencing and immunoblotting.

In KH2 cells, the knockout cell lines were generated as follows. KH2 cells carry the tetracycline responsive transactivator *M2-rtTA* at the *Rosa26* locus, which allows for doxycycline (Dox)-dependent expression of an exogenous gene [2]. *Cas9* cDNA was integrated into the *ColA1* locus of KH2 cells using a Flip-in vector containing the *IRES-mCherry* cassette as previously described [3].

Growth assay

Wild type and *Smarcb1*-knockout ESC lines were plated on 6-well plates at a density of 1×10^5 cells per well (Day 0). The number of cells was calculated at day 1, 2

and 3 using automatic cell counter TC10 (BioRad). The experiment was performed in biological triplicate.

Alkaline phosphatase staining

Alkaline phosphatase staining was performed with Alkaline Phosphatase Staining Kit (Stemgent) according to the manufacturer's instruction.

Western blotting

Feeder cells were removed by culturing in 2i/LIF ES medium which was supplemented with 1 μM PD0325901 (STEMGENT) and 3 μM CHIR99021 (STEMGENT) [4]. The suspension was centrifuged at 200g for 5 min. Cells were dissolved in 500 μl of RIPA lysis buffer containing protease inhibitor cocktail (Nacalai Tesque) and dithiothreitol (wako). A total of 30 μg denatured protein was run on 10% SDS–PAGE gels and transferred to Amersham Hybond-P PVDF Membranes (GE Healthcare) using PowerPac HC (Bio-Rad). Membranes were blocked with 4% skim milk (Nacalai Tesque) in 1 × TBS with 0.05% Tween-20 (TBST) and then incubated with primary antibodies diluted by blocking buffer (4% skim milk in TBST) overnight at 4 °C. The primary antibodies used were anti-INI1/SNF5 (Sigma-Aldrich:SAB4200202) and anti-β-actin (Santa Cruz, sc-47778). Membranes were rinsed with TBST. Membranes were incubated with HRP-conjugated secondary antibodies for 90 min at room temperature. The secondary antibodies used were ECL anti-mouse IgG, HRP-linked whole antibody from sheep (NA931V, GE Healthcare) and ECL anti-rabbit IgG, HRP linked whole antibody from donkey (NA934V, GE Healthcare). After membranes were rinsed with TBST, protein bands were visualized with Pierce ECL plus Western Blotting Substrate (Thermo Scientific) and detected by LAS4000 (GE Healthcare).

Immunocytofluorescence

Cells were fixed with PBS containing 2% paraformaldehyde (Wako) for 10 minutes, permeabilized with PBS containing 3% FBS and 0.1% Triton and stained with anti-CDX2 antibody (Thermo fisher, MA5-14494; dilution 1:200) and anti-OCT4 antibody (BD Transduction, 611203; dilution 1:200) overnight at 4 °C. Secondary antibodies conjugated with Alexa Fluor 594 (Invitrogen) and Alexa Fluor 488 (Invitrogen) and Hoechst 33258 (DOJINDO) were used for visualization. Immunofluorescence signals were detected by BZ-9000 (KEYENCE).

In vivo experiment

All animal experiments were approved by the CiRA Animal Experiment Committee and IMSUT Animal Experiment Committee, and the care of the animals was in accordance with institutional guidelines. ICR mice, pseudo-pregnant ICR mice and BALB/cSlc-nu/nu mice were purchased from SLC. Noon of the day when the plug was observed was designated as embryonic day E0.5. For teratoma formation, ESCs were trypsinized for single-cell suspension and 1×10^6 or 2×10^6 cells were injected subcutaneously into BALB/cSlc-nu/nu mice. Three weeks after the transplantation, formed teratomas were processed for histological analyses. For chimera formation, ESCs were labelled with EGFP by transfection with 2.5 μg of *piggyBac* (PB) transposon carrying *CAG-EGFP-IRES-Blast* using Xfect mES cell Transfection Reagent (Clontech). EGFP-labeled ES cells were injected into the E2.5 (8 cell) or blastocoels of E3.5 blastocysts. Injected blastocysts were transferred into the uteri of pseudo-pregnant ICR mice. Fluorescence Stereo Microscope Leica M205 FA (Leica MICROSYSTEMS), BZ-9000 (KEYENCE) or a confocal laser scanning microscope (Zeiss LSM700) was used for the observation of EGFP-labelled cells in embryos.

HE staining and immunohistochemistry

Samples were fixed with 4% paraformaldehyde overnight at room temperature and embedded in paraffin using Spin Tissue Processor STP120-2 (Thermo Scientific). Sections were stained with haematoxylin and eosin (HE). For immunohistochemistry,

sections were treated with xylene and 100% ethanol, then washed with water followed by treatment with Histofine (Nichirei). After rinsing with PBS, sections were incubated with anti-GFP antibody (Abcam, ab183734; dilution 1:200, Abcam, ab13970; dilution 1:500), anti-TPBPA antibody (Abcam, ab104401; dilution 1:200), anti-NESTIN antibody (BD, 611658; dilution 1:400) or anti-PL-1antibody (Santa Crus Biotechnology, sc-34713; dilution 1:150) overnight at 4 °C. Sections were then rinsed with PBS and incubated with Histofine Simple Stain Mouse MAX PO (Nichirei) containing secondary antibody for 30 min at room temperature. DAB Substrate Kit (Nichirei) was used for detection [5]. For immunofluorescence staining, anti-GFP antibody (Abcam, ab13970; dilution 1:500) and anti-TPBPA antibody (Abcam, ab104401; dilution 1:200) were used as primary antibodies. The sections were processed with fluorescence-labeled secondary antibodies and DAPI (Invitrogen, D21490; 1:500) for 90 min at room temperature. After washing in PBS for 5 min twice, immunofluorescence signals were detected by BZ-9000 (KEYENCE).

FACS sorting

For RNA-seq and ATAC-seq analyses, ESCs were sorted by a fluorescence activated cell sorter (FACS) Aria II (BD). Alexa Flour 647 conjugated anti-SSEA1 antibody (Santa Cruz, sc-21702 AF647 clone MC480 or BD Pharmingen, Clone MC480, cat: 562277) was used for the sorting. Sorted cells were used for RNA isolation and library preparation for next generation sequencing.

Quantitative RT-PCR

Quantitative RT-PCR was performed using GoTaq qPCR Master Mix and CXR Reference Dye (Promega) according to the supplier's instruction. StepOnePlus Real-Time PCR system (Applied Biosystems) was used. Transcript levels were normalized to β-actin (*Actb*). The primer sequences were:

Cdx2 forward : AGGCTGAGCCATGAGGAGTA;

Cdx2 reverse : CGAGGTCCATAATTCCACTCA;

Cited1 forward : AACCTTGGAGTGAAGGATCGC;

Cited1 reverse : GTAGGAGAGCCTATTGGAGATGT;

Hand1 forward : CCCCTCTTCCGTCCTCTTAC;

Hand1 reverse : CTGCGAGTGGTCACACTGAT;

Nanog forward : TGCTTACAAGGGTCTGCTACTG;

Nanog reverse : TAGAAGAATCAGGGCTGCCTTG;

Pou5f1 forward : TCCCATGCATTCAAACTGAG;

Pou5f1 reverse : CCACCCCTGTTGTGCTTTTA;

Sox2 forward : CCCACCTACAGCATGTCCTAC;

Sox2 reverse : GCCTCGGACTTGACCACAG;

Actb forward : GCCAACCGTGAAAAGATGAC; and

Actb reverse : TCCGGAGTCCATCACAATG

Library preparation for next generation sequencing

For RNA-seq, 200 ng of high-quality RNA (RNA Integrity Number value >=8) evaluated by Bioanalyzer (Agilent Technologies) was used for the library preparation. RNA-seq libraries were generated using Truseq Stranded mRNA LT sample prep kit (Illumina) according to the manufacturer's instructions. Resulting RNA-seq libraries were single-end sequenced with a length of 75 bp on NextSeq 500 (Illumina).

ATAC-seq libraries were prepared as previously described with some modifications [6]. Briefly, cells were collected by FACS with a SSEA-1 antibody (see the section above) and 50,000 cells were used to prepare nuclei. Cells were lysed with a lysis buffer (10mM Tris-HCl pH7.5, 3mM MgCl2, 10mM NaCl and 0.1% IGEPAL CA-630). Yielded nuclei were suspended in the transposase reaction mix (25 µl of 2X TD Buffer (Illumina), 2.5 µl of TD Enzyme 1 (Illumina), and 22.5 µl of nuclease-free water), and incubated for 30 minutes at 37 ℃ on a thermomixer shaker. Fragmented DNA was then purified using MinElute PCR purification kit (GIAGEN). After that, fragmented DNA was amplified by PCR to obtain ATAC-seq libraries. Resulting

libraries were purified using MinElute PCR purification kit, and quantified using KAPA Library Quantification Kit For Illumina (KAPA Biosystems). The libraries were paired-end sequenced with a length of 50 bp on Nextseq 500.

RNA-seq analysis

RNA-seq reads were aligned to the GENCODE version M17 annotation gtf file using STAR version 2.5.3a after trimming adaptor sequences and low-quality bases using cutadapt version 1.16 [7]. The number of reads which fell into each gene was counted using htseq-count version 0.9.1. The count data was then normalized using DESeq2 [8], and log2-transformed after adding pseudocount 1 to normalized count values. Reproducibility of the results of the RNA-seq analysis was confirmed by qPCR testing a couple of genes.

ATAC-seq analysis

Adaptor sequences in reads were trimmed using Trim Galore version 0.5.0 (http://www.bioinformatics.babraham.ac.uk/projects/trim_galore/). Then trimmed reads were aligned to the mm10 genome build using bowtie2 version 2.3.4.3 with default parameters except the --very-sensitive option, and filtered based on mapping scores (MAPQ ≥30) by samtools version 1.9 [9, 10]. Duplicated reads were removed using picard MarkDuplicates version 2.18.7. Reads mapped to regions blacklisted by ENCODE were removed with bedtools [11]. MACS2 version 2.1.2 was used to identify peaks in each sample with default settings [12]. All the peaks were then merged into a single reference peak list using bedtools merge, and the number of reads which fell into each peak was counted using bedtools multicov. Normalization of the count data were performed by using DESeq2. Motif analyses were performed using HOMER with default settings [13].

Data availability

All the RNA-seq and ATAC-seq data are available in SRA (BioProject:

PRJNA551543).

References

[1] L. Cong, F.A. Ran, D. Cox, S.L. Lin, R. Barretto, N. Habib, P.D. Hsu, X.B. Wu, W.Y. Jiang, L.A. Marraffini, F. Zhang, Multiplex Genome Engineering Using CRISPR/Cas Systems, Science, 339 (2013) 819-823.

[2] C. Beard, K. Hochedlinger, K. Plath, A. Wutz, R. Jaenisch, Efficient method to generate single-copy transgenic mice by site-specific integration in embryonic stem cells, Genesis, 44 (2006) 23-28.

[3] K. Ohnishi, K. Semi, T. Yamamoto, M. Shimizu, A. Tanaka, K. Mitsunaga, K. Okita, K. Osafune, Y. Arioka, T. Maeda, H. Soejima, H. Moriwaki, S. Yamanaka, K. Woltjen, Y. Yamada, Premature termination of reprogramming in vivo leads to cancer development through altered epigenetic regulation, Cell, 156 (2014) 663-677.

[4] M. Yagi, S. Kishigami, A. Tanaka, K. Semi, E. Mizutani, S. Wakayama, T. Wakayama, T. Yamamoto, Y. Yamada, Derivation of ground-state female ES cells maintaining gamete-derived DNA methylation, Nature, 548 (2017) 224-+.

[5] H. Shibata, S. Komura, Y. Yamada, N. Sankoda, A. Tanaka, T. Ukai, M. Kabata, S. Sakurai, B. Kuze, K. Woltjen, H. Haga, Y. Ito, Y. Kawaguchi, T. Yamamoto, Y. Yamada, In vivo reprogramming drives Kras-induced cancer development, Nat Commun, 9 (2018).

[6] J.D. Buenrostro, P.G. Giresi, L.C. Zaba, H.Y. Chang, W.J. Greenleaf, Transposition of native chromatin for fast and sensitive epigenomic profiling of open chromatin, DNA-binding proteins and nucleosome position, Nat Methods, 10 (2013) 1213-1218.

[7] M. Martin, Cutadapt removes adapter sequences from high-throughput sequencing reads, EMBnet.journal, 17 (2011).

[8] M.I. Love, W. Huber, S. Anders, Moderated estimation of fold change and dispersion for RNA-seq data with DESeq2, Genome Biol, 15 (2014) 550.

[9] B. Langmead, S.L. Salzberg, Fast gapped-read alignment with Bowtie 2, Nat Methods, 9 (2012) 357-359.

[10] H. Li, B. Handsaker, A. Wysoker, T. Fennell, J. Ruan, N. Homer, G. Marth, G. Abecasis, R. Durbin, S. Genome Project Data Processing, The Sequence Alignment/Map format and SAMtools, Bioinformatics, 25 (2009) 2078-2079.

[11] A.R. Quinlan, I.M. Hall, BEDTools: a flexible suite of utilities for comparing genomic features, Bioinformatics, 26 (2010) 841-842.

[12] Y. Zhang, T. Liu, C.A. Meyer, J. Eeckhoute, D.S. Johnson, B.E. Bernstein, C. Nusbaum, R.M.

Myers, M. Brown, W. Li, X.S. Liu, Model-based analysis of ChIP-Seq (MACS), Genome Biol, 9 (2008) R137.
[13] S. Heinz, C. Benner, N. Spann, E. Bertolino, Y.C. Lin, P. Laslo, J.X. Cheng, C. Murre, H. Singh, C.K. Glass, Simple combinations of lineage-determining transcription factors prime cis-regulatory elements required for macrophage and B cell identities, Mol Cell, 38 (2010) 576-589.

Figure S1

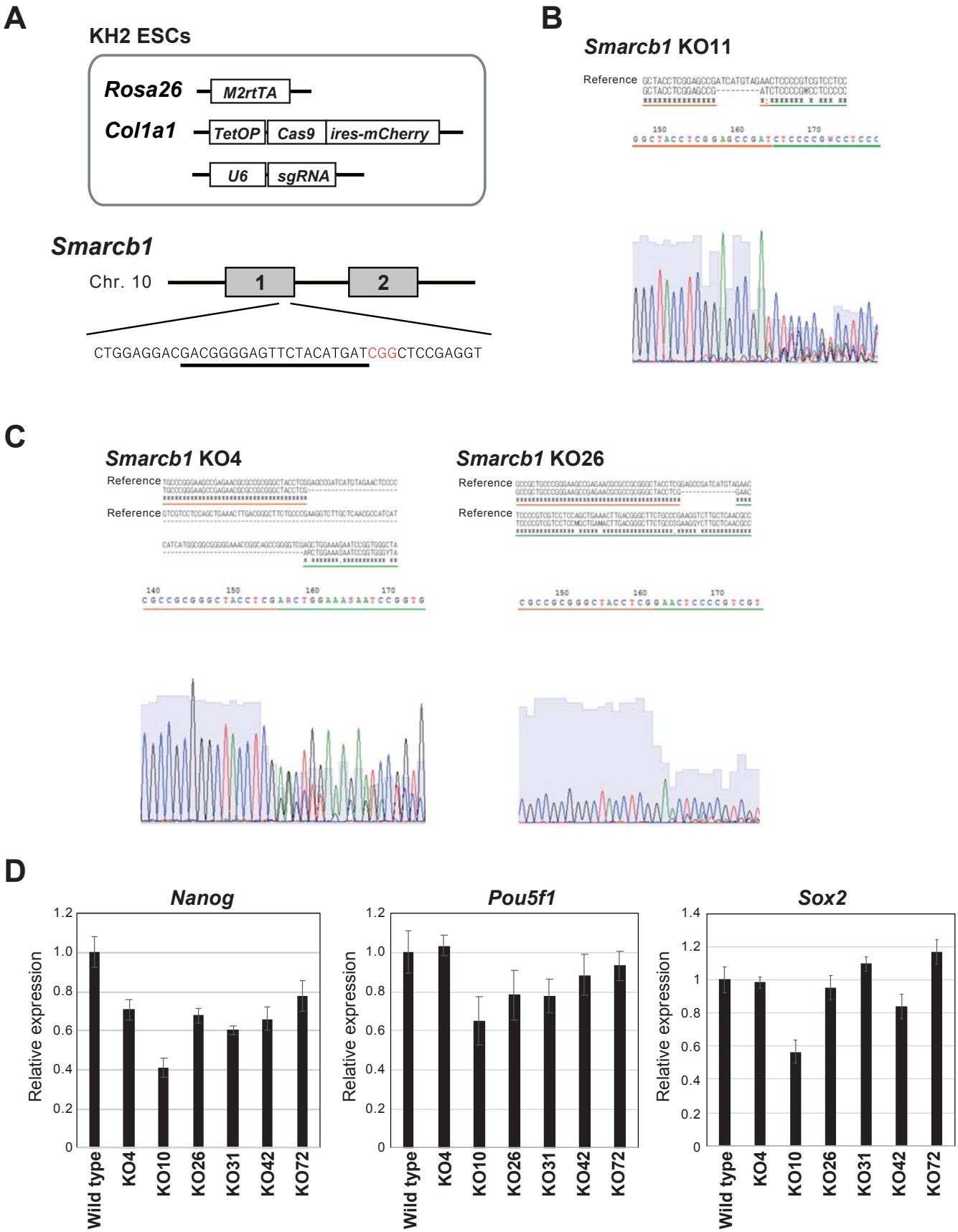
A
KH2 ESCs
Rosa26
M2rtTA
Col1a1
TetOP
Cas9
ires-mCherry
U6
sgRNA
Smarcb1
Chr. 10
1
2
CTGGAGGACGACGGGGAGTTCTACATGATCGGCTCCGAGGT
B
Smarcb1 KO11
Reference
C
Smarcb1 KO4
Reference
Reference
Smarcb1 KO26
Reference
Reference
D
Nanog
Pou5f1
Sox2
Relative expression
Wild type
KO4
KO10
KO26
KO31
KO42
KO72

Figure S1:

A: Strategy of knockout for *Smarcb1* using CRISPR/Cas9 in KH2 ESCs. sgRNA targeting sequence is underlined, and the PAM sequence is labelled in red.

B: Sanger sequencing revealed frameshift mutations in KH2 ESCs.

C: Sanger sequencing revealed frameshift mutations in V6.5 ESCs.

D: qRT-PCR analysis for *Nanog*, *Pou5f1* and *Sox2* in *Smarcb1*-deficient and control ESCs (V6.5). Data are presented as the mean ± SD of biological triplicates. The mean expression level of control ESCs was set to 1.

Figure S2

A

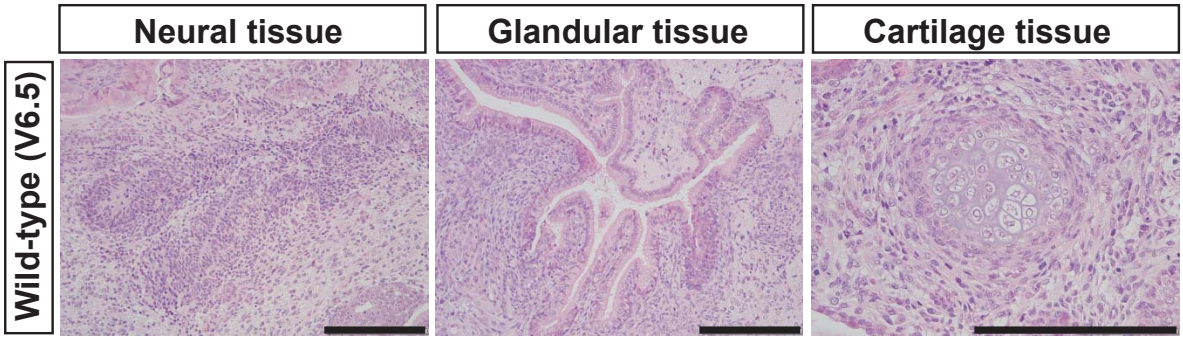
Neural tissue
Glandular tissue
Cartilage tissue
Wild-type (V6.5)

B

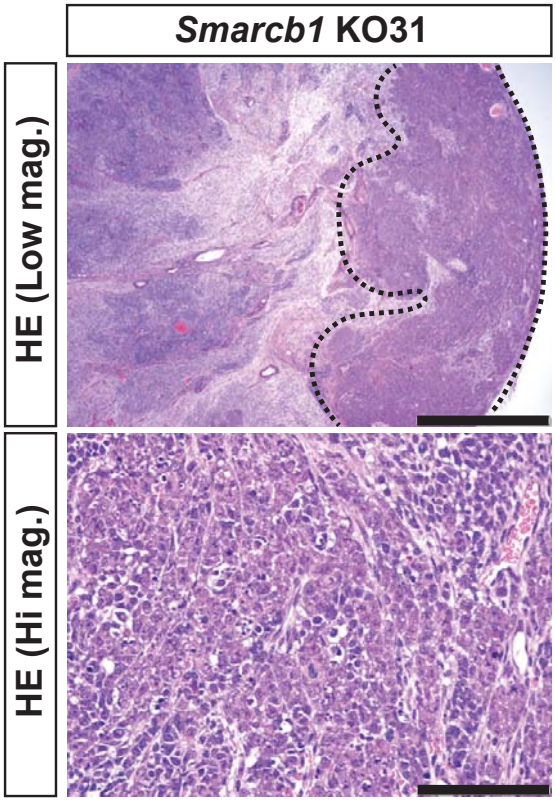
Smarcb1 KO31
HE (Low mag.)
HE (Hi mag.)

Figure S2:

A: Histology of wild type ESC (V6.5)-derived teratomas. Scale bars: 200 μm.

B: Dysplastic cell growth in the periphery of *Smarcb1* KO31-derived teratoma. Loss of SMARCB1 expression at the protein level is observed in almost all atypical teratoid/rhabdoid tumor (AT/RT), which is an extraordinarily lethal malignant CNS tumor that occurs mainly in early childhood. We observed the dysplastic cell growth in a *Smarcb1* KO31-derived teratoma. The dotted line outlines the dysplastic cell growth. The rhabdoid-like dysplastic cells display frequent mitotic figures. Scale bars: 1 mm (upper), 100 μm (lower).

Figure S3

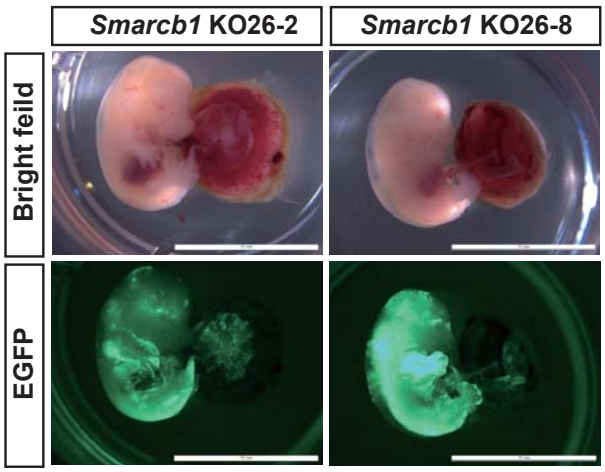

Figure S3:
EGFP images of the chimeric embryo and placenta at E14.5. Scale bars: 10 mm.

Figure S4

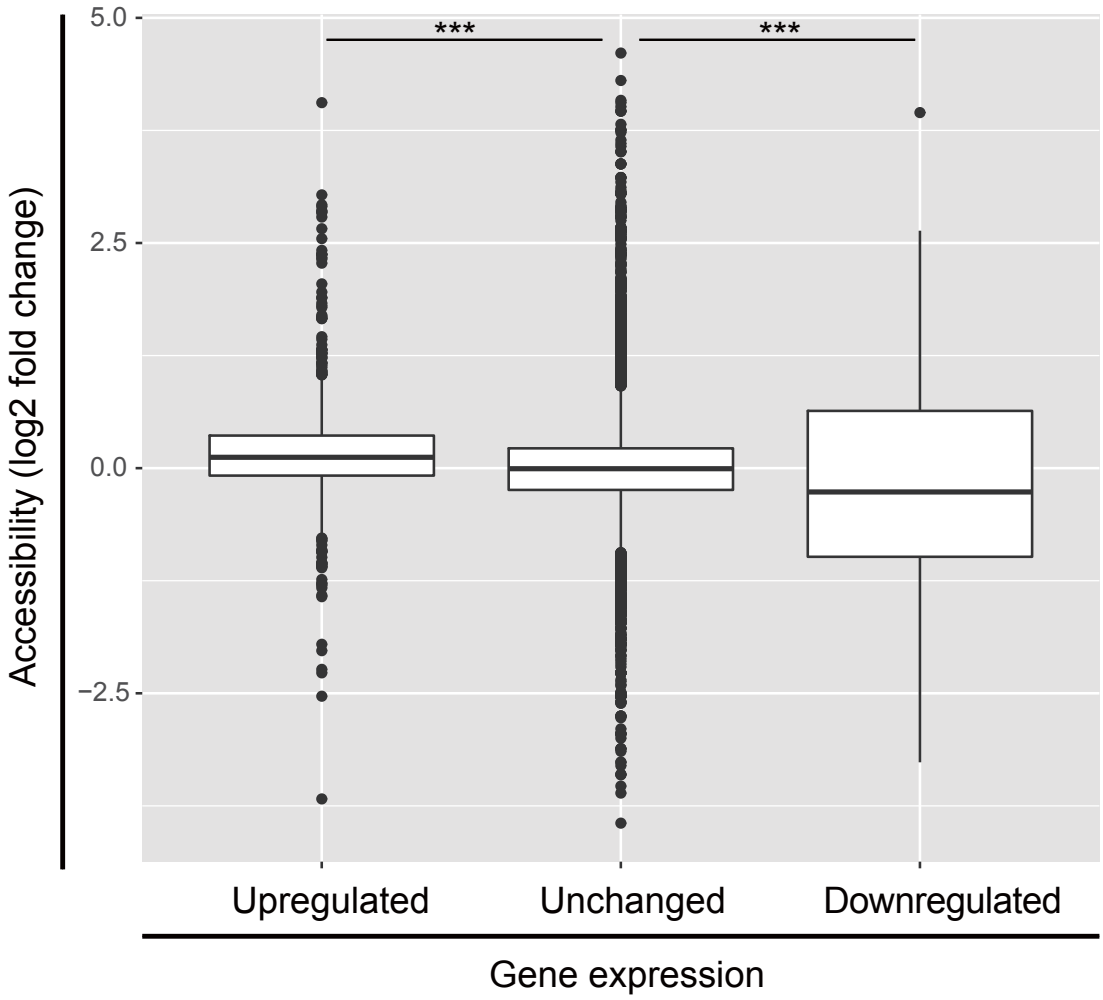
5.0
2.5
0.0
−2.5
***
***
Accessibility (log2 fold change)
Upregulated
Unchanged
Downregulated
Gene expression

Figure S4:
Correlation between changes in gene expression and those in accessibility of the promoter regions of the corresponding genes (***p<0.001, Wilcoxon rank sum test).